Australian Government
Department of Defence
Defence Science and
Technology Group

Satellite Laser Ranging Photon-Budget Calculations for a Single Satellite Cornercube Retroreflector: Attitude Control Tolerance

Philip C L Stephenson

National Security and ISR Division
Defence Science and Technology Group

DST-Group–TR–3172

ABSTRACT

The effect of cornercube retroreflector orientation on satellite laser ranging (SLR) detected photon counts is examined. It is found that a retroreflector tilt can ameliorate the effects of the satellite velocity aberration by broadening the reflected beam through diffraction. The optimal tilt angle, away from the SLR station, can be up to approximately 20.5° for the present retroreflector design. The size and direction of the tilt angle depend on the satellite velocity relative to the SLR station, and the direction of the satellite from the SLR station. The required attitude control tolerance is to within 17° of the optimal attitude control strategy determined in the present work. A pre-launch measurement of the reflectance (diffraction) pattern of each retroreflector is recommended to take account of the significant likely manufacturing variation.

Published by

National Security and ISR Division
Defence Science and Technology Group
PO Box 1500
Edinburgh, South Australia 5111, Australia

Telephone: *1300 333 362*
Facsimile: *(08) 7389 6567*

AR-016–445
November, 2015

APPROVED FOR PUBLIC RELEASE

Satellite Laser Ranging Photon-Budget Calculations for a Single Satellite Cornercube Retroreflector: Attitude Control Tolerance

Executive Summary

An early design study [1] in 2011 considered the suitability of a corner-cube retroreflector of radius 7.5 mm for a small-satellite mission. Some estimates of the laser beam transmitter and receiver optics were assumed, and pointing angles from the Zenith to 60° were considered. The retroreflector was found to give an adequate number of detected photons for a reasonable range of atmospheric conditions.

The present study concerns a smaller solid corner-cube retroreflector (with a radius of 6.35 mm) that has been adopted in the current satellite design. In particular, the study has concentrated on determining the tolerances on the retroreflector orientation.

The laser-beam transmitter and receiver optics parameter values have also been refined, as have the tolerances on pointing accuracy and these have been incorporated in the present study. These include a smaller beam divergence and greater pointing accuracy, but lower detector efficiency and optics transmittance and greater range of pointing angles (up to 75° from the zenith).

Two important aspects of the dependence of the detected photon count on the retroreflector orientation have been included in the present study that were omitted from the earlier work. The first is the shift in reflected beam angle due to the satellite speed; an effect known as the *velocity aberration*. In the present case, this causes a shift in beam direction of up to 11 arcsec. The size of the aberration depends on the angle between the satellite velocity and the direction from the satellite to the range station, and so varies with pointing angle. The second is the orientation dependence of the retroreflector diffraction pattern. This is a non-trivial exercise due to the complications involved in calculating the apparent aperture size of the retroreflector aperture. Most of the available literature concerns retroreflectors with a minimal depth-to-radius ratio (of 1.41), whereas the current retroreflector of interest has a larger ratio (1.85) and so the theoretical basis of the modelling has been re-derived.

It is found that the retroreflector should be tilted away from the SLR station in order to broaden the reflected beam by diffraction from a narrower aperture. This mitigates the effects of the velocity aberration. The optimum tilt angle varies with the size of the velocity aberration. At the maximum expected velocity aberration of 10.92 arcsec, a retroreflector tilt of $(20.5 \pm 17)^\circ$ is required to exceed the unity photon-count threshold, with a tilt of 20.5° being optimal. The axis of the rotation is perpendicular to both the satellite (relative) velocity and the direction to the SLR station.

The same tilt angle (and tolerance) can be used at lower velocity aberration values and still exceed the detection threshold. Nevertheless, a reduced tilt angle (according to the values in Table 2 and plotted in Figure 9) will give optimal photon counts.

The manufacturing tolerances of the cornercube retroreflectors identified in the current satellite design are found to allow for a significant variation in the reflected beam width. The possible diffraction patterns encompass a range of different attitude control strategies. It is likely that a different strategy will be required for each cornercube, depending on its particular diffraction pattern. It is even possible that some retroreflectors might not be suitable for use in the current application. It is therefore recommended that the pattern of each retroreflector be measured and an attitude control strategy developed to match each one.

Contents

Appendices

Figures

Tables

1 Introduction

The Biarri satellite will have a cornercube retroreflector mounted in its surface. This is to enable accurate ranging experiments to be performed on it using satellite laser ranging (SLR) techniques. The SLR will be conducted from Mount Stromlo in eastern Australia. An early design study [1], hereafter referred to as S&P, found that a single cornercube retroreflector with aperture radius of 7.5 mm would give a sufficient reflected signal for SLR using the transmission and receiving SLR equipment at Mount Stromlo.

The aim of the present work is to determine the attitude control necessary to ensure an adequate signal from the current retroreflector planned for the satellite. The signal is reduced if the retroreflector aperture is tilted away from the SLR station (hereafter referred to simply as the station) due to the smaller projected aperture area. There are other effects that also need to be considered. The diffraction pattern of the reflected light changes with retroreflector tilt, and an effect known as the velocity aberration will rotate the reflected distribution of light due to the satellite's high speed. These two effects are considered in some detail in the present work. It is found that there is an optimal, *non-zero* tilt of the retroreflector away from the direction to the station. This tilt angle depends on the satellite location (relative to the station), and the attitude tolerances are quite wide (of the order of 10°) if the detection threshold is to be met or exceeded.

There are two notable effects that have not been included in the present study. These are the effects of atmospheric turbulence on the propagation of the laser beam on both out- and in-bound journeys, and the sensitivity of the reflectivity of the cornercube faces to different states of the laser polarisation. The former will cause fluctuations in the signal strength, but are expected to preserve the average values calculated in the present work. The latter might be significant in some circumstances of retroreflector attitude where the reflection angles are high and there is an approximately 10% variation on reflectance between extreme states of polarisation [2]. These situations are expected to be transitory, and so not of significance in these photon-budget calculations where an average of the two reflectance values has been used.

2 SLR geometry and detection threshold

The geometry of the components of an SLR operation is illustrated in Figure 1. At the Mount Stromlo station the transmitter and receiver are co-located (sharing the same fore-optic) so that the receiver angle $\theta_r = \pm\alpha$, where the sign of the velocity aberration, α, depends on the direction of the satellite velocity (as discussed in §4.2.1). A laser beam pulse is sent from the transmitter toward the retroreflector and the time taken for the first return photon to be detected by the receiver is used to determine the distance travelled, and hence the range of the retroreflector. The pointing angle $\phi \leq 75^\circ$, and θ_i is the retroreflector tilt angle; the parameter of primary interest in the present work. The remaining parameters are defined and discussed at greater length in the following sections.

The details of how the pulse travel time is measured precisely is not of concern in the present work, which is focused mainly on modelling the strength of the return signal.

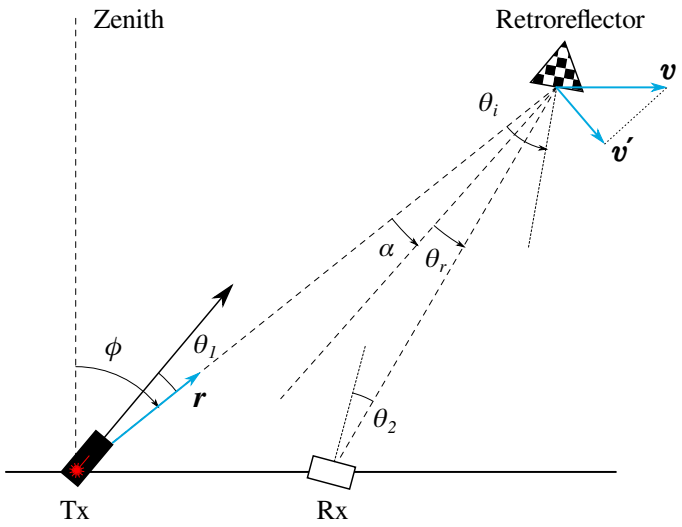

Figure 1: Diagram (not to scale) showing the angles defined for the satellite laser ranging geometry. The transmitter (Tx) and receiver (Rx) are in general separate (as shown), but in the present application will be co-located. The satellite—and hence the retroreflector—is moving with velocity $\boldsymbol{v}$ relative to the ground station. The velocity component normal to the displacement vector $\boldsymbol{r}$ between the transmitter and retroreflector is v'. The reflected light distribution is rotated through angle α by the effect known as the velocity aberration. If the transmitter and receiver are co-located then the receiver angle, $\theta_r = -\alpha$.

Nevertheless, it is worth noting that the detection of the return signal, and distinguishing it from background noise, is a statistical process that requires multiple pulses. The required minimum detectable photon count per pulse [3] is approximately $n_p \geq 0.02$ (2 photons per 100 pulses) at night and $n_p \geq 0.5$ (1 photon per 2 pulses) during daylight. For the current calculations a unity threshold ($n_p = 1$ photon per pulse) is therefore assumed, both for simplicity and to allow a margin of error for the many uncertain variables involved, such as the atmosphere.

3 Retroreflector design

The retroreflector planned to be used on the satellite is a solid, crown-glass cornercube with silvered reflecting surfaces. It is an off-the-shelf item from a large, optical-component manufacturing company. The retroreflector design parameter values are listed in Figure 2. The crown-glass material N-BK7 has a refractive index [2] $n = 1.519$ at the wavelength ($\lambda = 532$ nm) used for SLR from Mount Stromlo. The surface silvering improves the reflectance over uncoated glass surfaces. It is assumed in the present study that the reflectance of the silver coating will be equal to that of silver metal (0.95) [2], giving a nett three-surface reflectance for the cornercube of $\rho = 0.857$. The circular aperture (radius $r_{cc} = 6.35$ mm) of the retroreflector is not recessed in its holder or the satellite. This is important in determining its reflective area at oblique ranging angles, and its consequent reflected diffraction pattern.

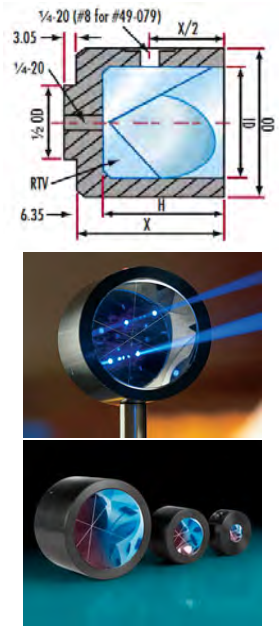

Edmund Optics #45-203	
Outer diameter, OD†	31.75 mm
Inner diameter, ID ($= 2r_{cc}$)	12.70 mm
Height, H ($= l$)	11.73 mm
Length, X†	18.08 mm
Diameter tolerance	$+0/-1$ mm
Surface accuracy	$1/8\ \lambda$
Surface quality	60-40
Housing tolerance	OD:† $+0/-0.5$ mm
	H: ± 0.25 mm
Beam-angle tolerance	3 arcsec
Substrate	N-BK7
Coating	Internal silver

Figure 2: Design diagram, representative photographs, and a list of physical properties of the retroreflector solid cornercube under consideration (from [4]). The quantities marked "†" do not directly affect optical performance.

3.1 Cornercube retroreflector dihedral angle tolerance

The reflected diffraction pattern from a cornercube retroreflector depends critically on the sizes of the three dihedral angles between the reflecting faces. If these angles are exactly right angles, then the narrow-beam (that is, without the diffraction-broadening effects) reflected direction will be exactly the opposite of the incoming beam, as required. Offsets in these dihedral angles will in general lead to a deviation from the ideal return beam direction. As is often the case, the present cornercube retroreflector design specifies a tolerance on the return-beam direction (up to 3 arcsec $\approx$ 15 μrad) rather than the dihedral angle tolerances. The dihedral angle tolerance can nevertheless be inferred from the reflected angle tolerance, and this has been done in Appendix B. It is found that the corresponding dihedral angle tolerance is ± 1.2 arcsec (or ± 5.8 μrad), for a cornercube of this material and geometry. Note that the unit of arcsec is used throughout this work for specifying the size of small angles, as is usual in the field of SLR. The approximate conversion to μrad is possible simply by multiplying by a factor of 4.85.

The return SLR laser beam can be broadened (or narrowed) in different directions by changing the dihedral angles. Broadening the return beam will lower its radiance, but often this penalty is outweighed by the benefit of mitigating the beam deflection away from the SLR receiver due to the velocity aberration, discussed below. Often, satellite retroreflectors will be intentionally adjusted (known as *spoiling*) in this way. Typically, the amount of spoiling will be less than approximately 2 arcsec [5]. The spoiling might be applied equally to all the dihedral angles for a more-or-less rotationally symmetrical change in beam width, or different amounts applied to each angle for preferential broadening in some directions but not others. Otsubo [6] gives examples of spoiling of

0.35 arcsec that broadens (or reduces, depending on whether it is applied to all angles or not) the beam width by a factor of two.

The retroreflectors of the current design therefore have a dihedral angle tolerance that could lead to spoiling that profoundly affects their performance (one way or another) in SLR. In the present work, a perfect geometry is assumed in order to determine a baseline attitude control strategy. It is nevertheless recommended that the far-field diffraction pattern of each retroreflector be characterised experimentally in order to determine its optimal attitude control strategy due to the potential for significant differences due to the actual detailed cornercube geometry of the retroreflectors. An industry-standard method for testing space retroreflectors is described by Boni *et al.* [7] and by Dell'Agnello *et al.* [8]. The method uses a laser-beam profiler, beam splitter, and an arrangement of polarising prisms and waveplates to measure the diffraction pattern resulting from uniform laser beams in different polarisation states. A different wavelength laser light is used in those works from the present SLR station, although this need not be the case. If a different wavelength is used, the diffraction pattern will be different, and adjustments to the measured reflectance pattern would need to be made in order to predict the actual SLR reflectance pattern. This could be done using the simulation methods developed, for example, by Arnold [9].

4 Radar link equation

The number, n_p, of photons detected at an optical receiver, from a laser source after reflection from a (distant) satellite, is often calculated using an expression from the theory of radar called the *radar link equation*. This expression includes the effects of losses within the transmitting and receiving optics, losses during the journey of the beam through the atmosphere in both directions, and the effects of beam broadening on both the outward and return paths. The present work follows the methods outlined in the review article by Degnan [5].

The radar link equation for the number of detected photons can be written as

$$n_p = \frac{E_t \lambda}{hc} \eta_t \frac{G_T}{4\pi d^2} \frac{\sigma}{4\pi d^2} A_r \eta_r \eta_q T_a^2 T_c^2. \tag{1}$$

Here the first term accounts for the number of photos emitted during a pulse of the laser source of energy E_t and wavelength λ, with h the Plank constant and c the speed of light in a vacuum. The efficiency, η_t, of the transmitting optics accounts for losses within the broadcasting telescope.

The reduction in the irradiance, due to broadening, of the beam on its path of length d (also known as the range) to the retroreflector is given by the term $G_T/(4\pi d^2)$ where the gain, G_T, is a function of beam divergence and direction, as discussed below. Similarly, the effect of the divergence of the light reflected from the satellite (retroreflector) is described by the subsequent term, where σ is the optical cross section of the retroreflector. The optical cross section is due to the finite retroreflector area presented to the incoming beam and the effects of diffraction of the light, and so depends on both the orientation of the retroreflector, and the direction of the receiver.

The return path to the receiver is assumed to be of equal length, d, to that of the outward path. During the double crossing of the Earth's atmosphere, a proportion of the light will be lost through absorption and scattering. This is accounted for by the transmittances T_a and T_c through the atmosphere and cirrus clouds respectively.

The receiver will have receiving optics of area A_r and receiving optics efficiency η_r, while the efficiency of the detector itself is η_q.

Expressions for the gain, G_T, and the retroreflector optical cross section, σ, were given in S&P [1], and are summarised below. Values for the atmospheric transmittance, T_a, and the cirrus-cloud transmittance, T_c, were also calculated for a range of likely scenarios. The present work largely concerns the retroreflector optical cross section, or gain, σ, its variation with the retroreflector orientation, and the effect this has on the final photon count at the receiver.

4.1 Transmitter gain

The transmitter gain depends on the propagation characteristics of the laser beam; which in turn depend on the transmitter optics, aperture size, beam divergence and beam profile. These are considered below for the present application of satellite laser ranging where the laser beam has a top-hat beam profile. In this case the Fresnel-Kirchhoff diffraction integral can be used to derive an expression for the gain [10, 11]. If the aperture inner and outer radii are respectively b and a, and if the radius of curvature of the wavefront at the aperture is again R, then the gain

$$G_T = \frac{4\pi}{\lambda^2(1-\gamma^2)^2}\left|\int_{\gamma^2}^{1}\exp[i\beta u]J_0(X\sqrt{u})\,du\right|^2, \tag{2}$$

where J_0 is a Bessel function of the first kind, u is the normalised radial distance on the laser aperture, $\gamma = b/a$, $X = ka\sin\theta_1$, θ_1 is the angle from the central axis of the beam—in the present case, the pointing error of the laser—and

$$\beta = \frac{ka^2}{2}\left(\frac{1}{d}+\frac{1}{R}\right). \tag{3}$$

The (slant) range, d, is calculated assuming a circular satellite orbit of altitude $h_s = 600$ km, about the Earth of radius $R_e = 6.378\times10^3$ km. For a pointing angle of ϕ from the zenith, the range is

$$d = \sqrt{R_e^2\cos^2\phi + 2R_eh_s + h_s^2} - R_e\cos\phi \tag{4}$$

from simple trigonometry. Note that no account of atmospheric refraction has been made in this approximation. Typically, the error is not greater than 10 m [5] and so can be safely neglected when calculating return pulse strength.

If the beam divergence is again denoted θ_d, then the wavefront radius of curvature at the aperture can be calculated using straightforward trigonometry as

$$R = \frac{a}{\tan\frac{\theta_d}{2}}. \tag{5}$$

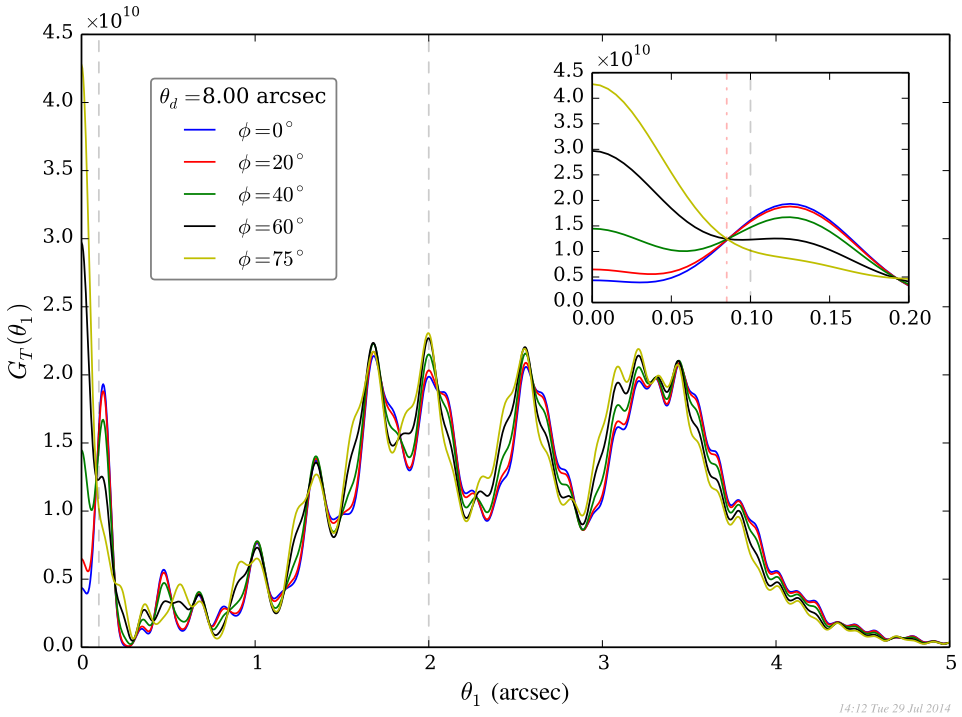

Figure 3: Transmitter gain, $G_T(\theta_1)$ with angle, θ_1, of the laser beam direction error. Values of the beam pointing accuracy metrics (the relative and absolute rms pointing accuracies) are shown as vertical dashed grey lines. The dashed-dotted red line shows the angle of stationary gain, $\theta_1 = 0.085$ arcsec. The gain for a selection from the allowed range of satellite zenith angles, ϕ, and therefore distances, d, are shown.

A positive value of R corresponds to a diverging beam, while a negative value corresponds to a converging beam.

The resulting gain is plotted as a function of beam direction in Figure 3 for a range of pointing angles (and therefore of satellite ranges). The relative and absolute rms pointing accuracies of the station are 0.1 arcsec and 2 arcsec, respectively, are indicated in the figure. The magnitude of the central bright spot ($\theta_1 \lesssim 0.08$ arcsec) and first lobe ($\theta_1 \lesssim 0.2$ arcsec) can be seen to vary by a factor of approximately 10 and 2, respectively, over the range of target distances. The rest of the distribution is nevertheless relatively stable. The effects of atmospheric turbulence on coherent-beam propagation is too complex to be considered in any detail in the present work. Degnan [5] states that the resulting beam-broadening is likely to be minimal in most cases, being not greater than a few percent. Beam wander and scintillation of the beam will be apparent as fluctuations in the signal strength, without a change in the mean value. The values of the gain at a beam pointing error, θ_1, of 0.085 arcsec can be seen not to vary with satellite direction, ϕ, from the zenith. This value of beam pointing error is close to the relative rms pointing accuracy. So the transmitter gain at this angle ($G_T(0.085) = 1.25 \times 10^{10}$) is taken as a representative worst-case value in the remainder of the present work.

4.2 Retroreflector optical cross-section

As shown in S&P [1], the retroreflector optical cross-section, σ, in the far-field limit, $r_{cc}/d \to 0$, can be written

$$\sigma = \rho \frac{4\pi A_{cc}^2}{\lambda^2} \left[\frac{2J_1(kr_{cc} \sin\theta_r)}{kr_{cc} \sin\theta_r} \right]^2, \tag{6}$$

when the retroreflector is oriented normal to the incident light, and where θ_r is the receiver orientation error (see Figure 1), ρ is the retroreflector reflectance (or efficiency), J_1 is a Bessel function of the first kind, k is the propagation number $2\pi/\lambda$, and $A_{cc} = \pi r_{cc}^2$ is the area of the retroreflector circular aperture of radius r_{cc}. The optical cross-section for on-axis (that is, when $\theta_r = 0$) reflected light will therefore be

$$\sigma\Big|_{\theta_r=0} = \rho \frac{4\pi}{\lambda^2} A_{cc}^2 \tag{7}$$

which can be seen to be proportional to the square of the retroreflector aperture area. Light at other reflection angles is distributed according to the Airy diffraction pattern as described above in equation (6).

For on-axis reflected light, when the retroreflector is a corner cube, and is not oriented normal to the incident light but at an angle θ_i from the normal, the area A_{cc} in the above expression (7) must be reduced by the factor [12, 5] (and see Appendix A)

$$\kappa(\theta_i) = \frac{2}{\pi} \left[\sin^{-1}\mu - (l/r_{cc})\mu \tan|\theta'| \right] \cos\theta_i, \tag{8}$$

where θ' is the refracted angle in the corner cube given by Snel's law of refraction

$$n \sin\theta' = \sin\theta_i, \tag{9}$$

where n is the cube index of refraction, and where

$$\mu = \sqrt{1 - (l/r_{cc})^2 \tan^2\theta'} \tag{10}$$

is the normalised reduced aperture radius along the tilt direction. The variation of the optical cross-section (on axis) with retroreflector angle is therefore $\kappa^2(\theta_i)$. This function is shown plotted in Figure 4 for the present case of a retroreflector made of BK7 crown glass. Its values are tabulated in Table 1. The cornercube ratio l/r_{cc} is an important parameter of the retroreflector. It is the ratio of the depth, l, of the cornercube to its aperture radius, r_{cc}. For a fully circular aperture, the ratio must be at least $\sqrt{2}$, but is often larger than this in order to avoid thin edges. The apparent aperture area decreases with tilt angle most slowly in cornercubes with this minimum-value ratio

$$(l/r_{cc})_{\text{min}} - \sqrt{2} \tag{11}$$

as shown in Figure 4. When this ratio is larger, as in the present case, the fall-off is more rapid, and such retroreflectors are more sensitive to the effects of tilting.

More generally the optical cross-section off-axis is broadened in one direction by the narrower effective aperture in the direction of the tilt. In this case the optical cross-section

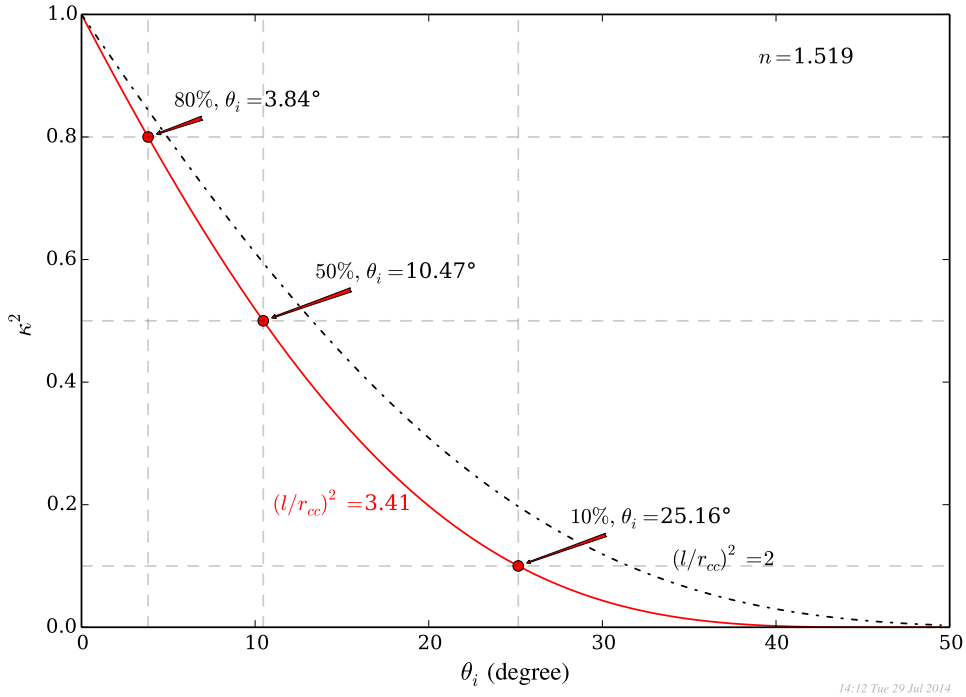

Figure 4: On-axis retroreflector optical cross-section variation, $\kappa^2(\theta_i)$ with angle, θ_i, of the retroreflector axis from the incident beam direction. The plot shows the case of a solid retroreflector constructed of BK7 crown glass with refractive index $n = 1.519$. Values of the angle θ_i are shown where the gain has reduced to 80%, 50% and 10% of its maximum value.

is more difficult to calculate because of the more complex aperture shape in the diffraction integral. The method of calculation is described in Appendix A and the resulting expression for the optical cross-section is

$$\sigma = \rho \frac{4\pi}{\lambda^2} \frac{A_{cc}^2}{\pi^2} W^2(x, y) \tag{12}$$

where $W(x, y)$ is defined by equation (A11) but calculated using equations (A16) and (A17). On axis, note that

$$W(0, 0) = \pi\kappa(\theta_i) \tag{13}$$

as expected. Off axis, the effects of the tilted retroreflector are illustrated in Figure 5. The optical cross-section can be seen to broaden in the same direction that the effective aperture width is reduced, as discussed in Appendix A. The overall magnitude of the optical cross-section is reduced, in accordance with the variation of $\kappa^2(\theta_i)$, in the on-axis ($\theta_r = 0$) direction.

4.2.1 Velocity aberration

As the receiver is co-incident with the transmitter optics, one might expect the appropriate value for the reflected light angle, θ_r, in the radar equation to be zero. Indeed,

Table 1: Retroreflector optical cross-section variation, $\kappa^2(\theta_i)$, tabulated as a function of angle, θ_i, of the retroreflector axis from the incident beam direction. In this case the retroreflector is made of solid BK7 crown glass with refractive index $n = 1.519$.

$\theta_i(^\circ)$	κ^2	$\theta_i(^\circ)$	κ^2	$\theta_i(^\circ)$	κ^2	$\theta_i(^\circ)$	κ^2	$\theta_i(^\circ)$	κ^2
0.0	1.000	6.0	0.695	12.0	0.441	18.0	0.248	24.0	0.118
0.5	0.973	6.5	0.672	12.5	0.422	18.5	0.235	24.5	0.110
1.0	0.946	7.0	0.649	13.0	0.404	19.0	0.222	25.0	0.102
1.5	0.920	7.5	0.626	13.5	0.387	19.5	0.210	25.5	0.095
2.0	0.894	8.0	0.604	14.0	0.369	20.0	0.198	26.0	0.088
2.5	0.868	8.5	0.582	14.5	0.353	20.5	0.187	26.5	0.081
3.0	0.842	9.0	0.561	15.0	0.336	21.0	0.176	27.0	0.075
3.5	0.817	9.5	0.540	15.5	0.321	21.5	0.165	27.5	0.069
4.0	0.792	10.0	0.519	16.0	0.305	22.0	0.155	28.0	0.063
4.5	0.767	10.5	0.499	16.5	0.290	22.5	0.145	28.5	0.058
5.0	0.743	11.0	0.479	17.0	0.276	23.0	0.136	29.0	0.053
5.5	0.719	11.5	0.460	17.5	0.262	23.5	0.127	29.5	0.048

this would be correct if the target (satellite) were stationary relative to the transmitter/receiver station. Yet the relative velocity of the satellite is in general non-zero, and this causes a small, but in many cases significant, change in the apparent direction of the laser beam—known as the velocity aberration [5, 13]. Denoted by α, the aberration causes a change in the receiver angle $\theta_r = \alpha$ as illustrated in Figures 6 and 1. As shown below, the magnitude of the aberration can be as large as approximately 11 arcsec; comparable to the width of the reflected beam, so the effect is significant.

The velocity of the satellite is sufficiently large (≈ 7.5 km/s) to affect appreciably the apparent angle at which the laser beam strikes it. If the component of the satellite relative velocity, $\boldsymbol{v}$, that is orthogonal to the direction to the station is denoted $\boldsymbol{v}'$, then the change in angle is [14] $\tan^{-1}(v'/c)$ by the classical (Bradley) approximation, which holds when $v' \ll c$ where c is the speed of light. The reflected beam will undergo a similar perceived rotation in the station frame of reference, and so the total angular shift—or velocity aberration—will be

$$\alpha = 2\tan^{-1}\left(\frac{v'}{c}\right) \approx \frac{2v'}{c}. \tag{14}$$

This first-order approximation is sufficiently accurate for satellite speeds, where the second-order terms have been shown [13] to be approximately 10^{-4} times smaller.

The speed of a satellite in a circular orbit can be simply calculated from its altitude, h_s, as

$$v = \sqrt{\frac{R_e^2 g}{R_e + h_s}} \tag{15}$$

where R_e is the radius of the Earth and g is the acceleration due to gravity. It can be shown [15, 5] that the velocity aberration is

$$\alpha(\phi, \omega) = \alpha_m \sqrt{\cos^2\omega + \Gamma^2(\phi)\sin^2\omega} \tag{16}$$

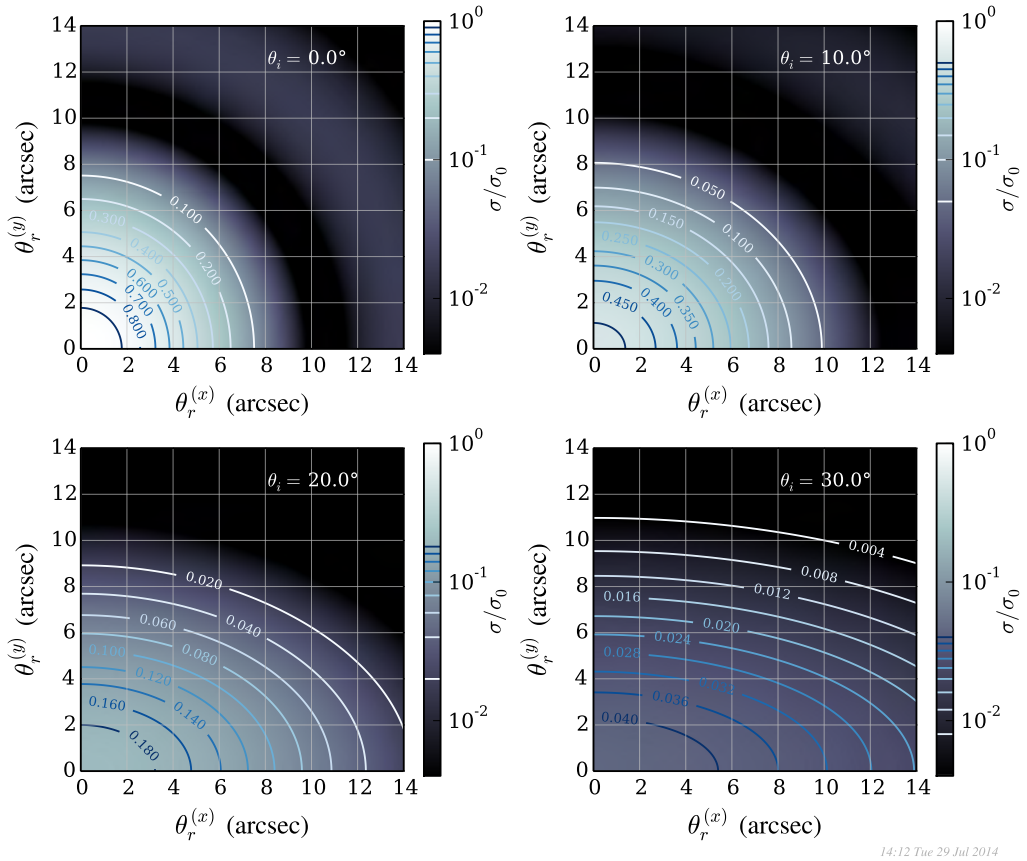

Figure 5: Normalised optical cross-section, σ/σ_0, as a function of reflected angles $\theta_r^{(x,y)}$ defined by $(x, y) = d \tan \theta_r^{(x,y)}$. False-colour plots corresponding to each of four tilt angles, θ_i, of the retroreflector about an axis parallel to the y-axis are shown. Broadening of the diffraction pattern along the x-axis can be seen, accompanied by an overall reduction in magnitude according to $\kappa^2(\theta_i)$ on axis ($\theta_r^{(x)} = \theta_r^{(y)} = 0$).

where ϕ is the transmitter pointing angle from the zenith, the quantity Γ varies with pointing direction and is given by

$$\Gamma(\phi) = \sqrt{1 - \left(\frac{R_e \sin\phi}{R_e + h_s}\right)^2}, \tag{17}$$

and ω is the azimuthal angle of the satellite velocity in the plane orthogonal to the position vector, $\boldsymbol{r}$, of the satellite relative to the station. The angle ω can be shown to be

$$\omega = \cos^{-1}[(\hat{\boldsymbol{r}} \times \hat{\boldsymbol{s}}) \cdot \hat{\boldsymbol{v}}] \tag{18}$$

where $\boldsymbol{s}$ is the position vector of the satellite relative to the centre of the Earth, and "$\hat{\cdot}$" indicates a unit vector. The velocity aberration therefore varies between the two extremes

$$\alpha_{\max} = \alpha_m \tag{19}$$

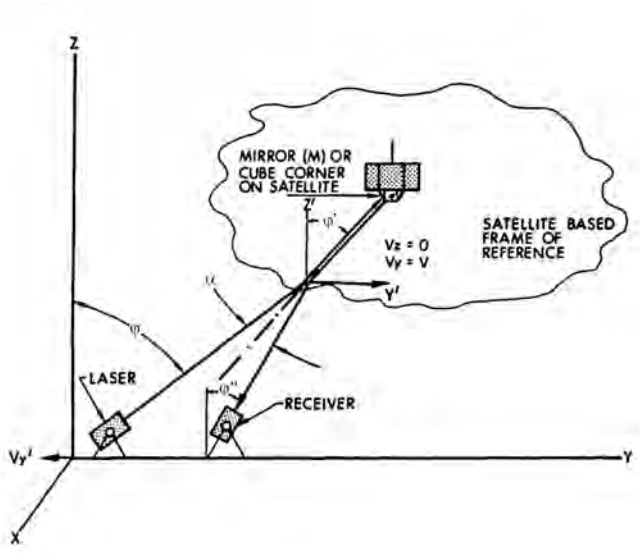

Figure 6: Diagram illustrating the beam directions in both the ground- and satellite-based frames of reference that account for the velocity aberration, α, in the reflected light distribution. Figure taken from [13].

and

$$\alpha_{\text{min}} = \alpha_m \Gamma(\phi) \tag{20}$$

for a given pointing angle ϕ, and where the maximum aberration, α_m, depends on the speed and can be expressed as

$$\alpha_m = \frac{2v}{c}. \tag{21}$$

If the rotation of the Earth—and hence the velocity of the station, $\bar{v}$—is taken in to account, then for a general orbit path the two extremes become

$$\alpha_{\text{max}} = \frac{2(v + \bar{v})}{c} = \alpha_m + \frac{2\bar{v}}{c}, \tag{22}$$

and

$$\alpha_{\text{min}} = \frac{2(v\Gamma(\phi) - \bar{v})}{c} = \alpha_m \Gamma(\phi) - \frac{2\bar{v}}{c}. \tag{23}$$

The station speed depends on its latitude, φ, and is, from simple geometry,

$$\bar{v} = \frac{2\pi R_e \cos\varphi}{T_{\text{day}}} \tag{24}$$

where T_{day} is the length of one day.

These limits to the range of the velocity aberration for a satellite in a 600 km orbit, and a station at Mount Stromlo, are plotted in Figure 7 as a function of pointing angle. The maximum velocity aberration, α_m, is the same at all pointing angles and is equal to 10.92 arcsec (52.9 μrad). The minimum varies with pointing angle, from its largest at zenith down to $\alpha_{\text{min}} = 4.4$ arcsec (21.3 μrad) at 75° from the zenith.

This range of velocity aberrations applied to the current-design retroreflector optical cross section can be seen in Figure 8. The unity photon-count threshold is also shown, and was

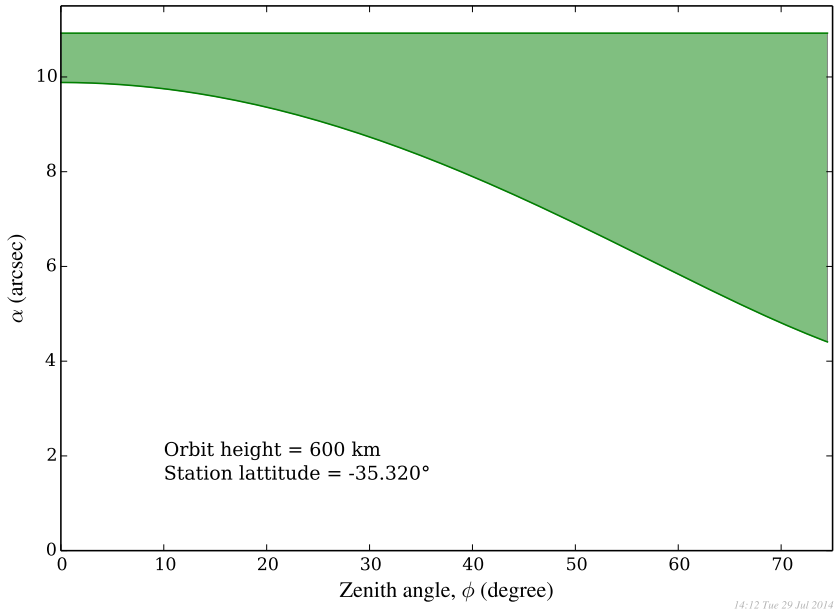

Figure 7: Velocity aberration, α, range (shaded) as a function of pointing angle for an orbit height of 600 km. The range includes the effects due to a circular satellite orbit, and the speed of the station due to the rotation of the Earth.

calculated by inverting the radar link equation (1) with the photon count $n_p = 1$, and worst expected-case parameter values used for the transmitter gain, transmittance and range; that is, $\theta_1 = 0.1$ arcsec and $\phi = 75°$. This threshold will therefore be lower in more favourable circumstances. It can be seen from this figure that the presence of the larger velocity aberrations will cause the minimum of the diffraction pattern of the retroreflector directed at the station to coincide with the receiver, and so the photon count to fall below the required unity threshold.

There is more than one way to address this problem. Very often retroreflectors are *spoiled* to broaden the reflected light preferentially to the angles θ_r close to the range of expected velocity aberration α. Spoiling is the term used to describe a cornercube retroreflector design with faces meeting at angles slightly perturbed ($\lesssim 2$ arcsec) from the usual right-angles [5, 6]. This approach is not possible in the present project.

An alternative is to use a retroreflector with a smaller aperture, and hence a broader diffraction pattern whose minima fall outside the range of velocity aberration angles. The diffraction pattern of just such a retroreflector is plotted in Figure 8. Although this does increase the optical cross section above the critical threshold where required, it reduces its value considerably in other regions and places greater constraints on the range of acceptable tilt angles; requiring greater satellite attitude control.

The final, and preferred, option is to broaden the diffraction pattern of the existing retroreflector by tilting it to achieve a narrower effective aperture in the same direction as the velocity aberration. If the normal to the retroreflector aperture is tilted as an angle θ_i

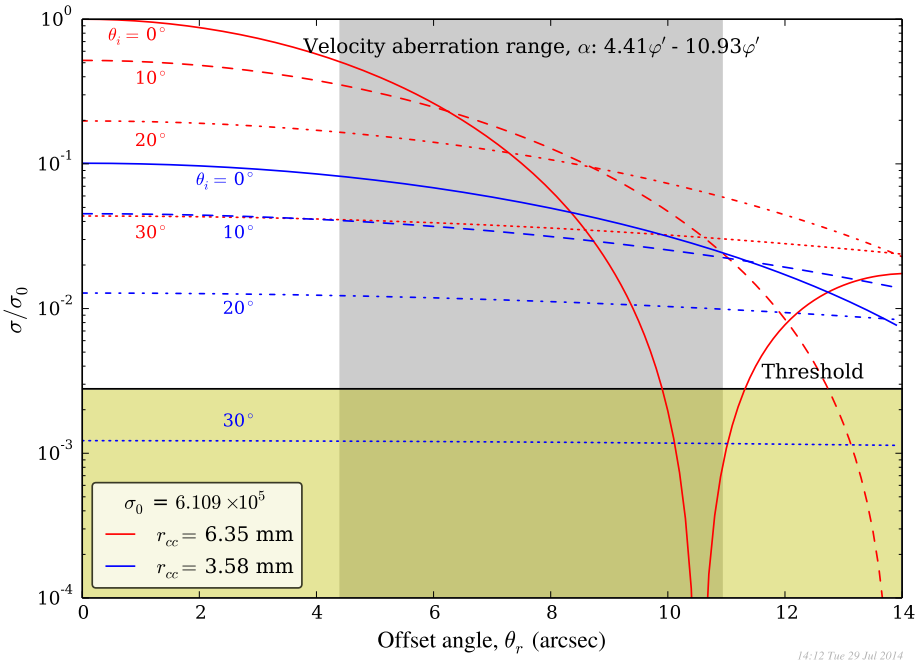

Figure 8: Normalised retroreflector optical cross section, σ/σ_0, as a function of receiver angle, θ_r, for a range of retroreflector tilt angles and two aperture sizes. The range of applicable receiver angles due to the velocity aberration is shaded grey. The unity photon-count threshold is shown shaded yellow.

away from the station, and in the direction of the projected relative satellite velocity

$$\boldsymbol{v}' = [\boldsymbol{v} - (\boldsymbol{v} \cdot \hat{\boldsymbol{r}})\hat{\boldsymbol{r}}] \tag{25}$$

then the diffraction pattern is broadened in the direction of the velocity aberration. In this way the optical cross section in increased above the threshold where (and when) required.

The optimal tilt angle, $\theta_i^{(o)}$, can be found for any given velocity aberration by numerically maximising the optical cross section with respect to θ_i. The optimal angle will, in general, vary with the velocity aberration, α. The resulting function, $\theta_i^{(o)}(\alpha)$, is plotted in Figure 9. For velocity aberrations α below approximately 5.5 arcsec, any increase in the optical cross section due to beam broadening with tilt is insufficient to compensate for the accompanying reduction in the optical cross section due to the reduced effective retroreflector area presented to the laser beam. In these cases, directing the retroreflector aperture directly at the station is optimal; that is, when $\theta_i = 0$. By contrast, at higher velocity aberration values, tilting the retroreflector is advantageous. For example, when the velocity aberration is its highest (for the present orbit) $\alpha = \alpha_{\text{max}} = 10.92$ arcsec, the optimal tilt angle $\theta_i^{(o)} = 20.5°$, and the range of tilt angles for which the optical cross section exceeds the unity photon-count threshold is quite wide; namely, $5° \leq \theta_i \leq 39°$. If necessary, a tilt angle within this range centred at $\theta_i = 20.5°$ could be maintained for any velocity aberration value, and the resulting optical cross section would remain above

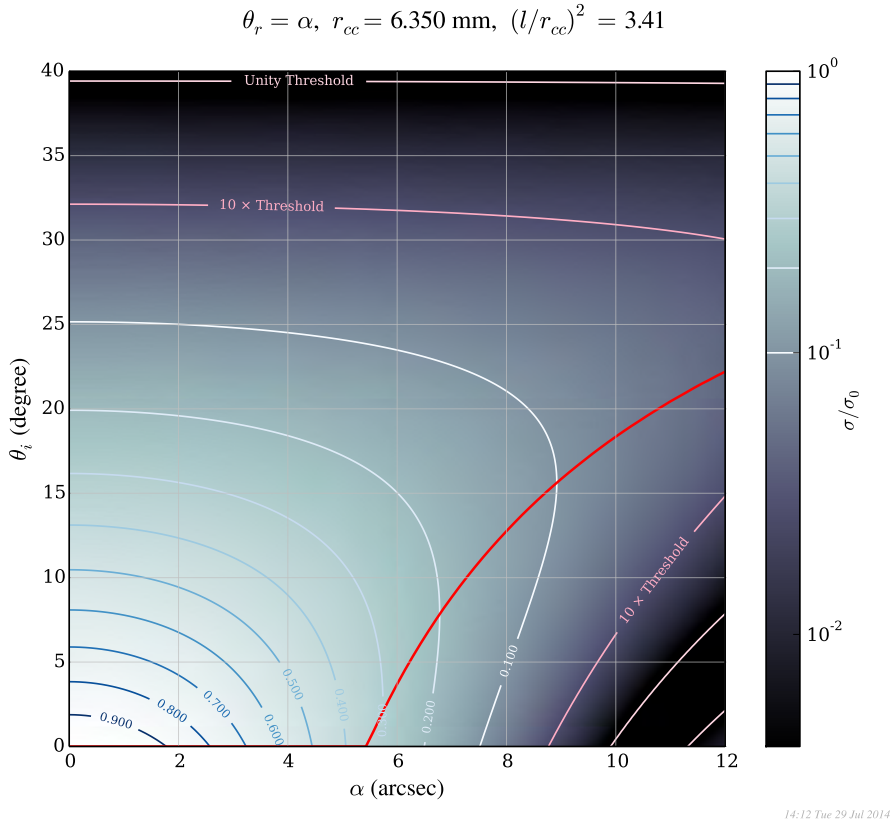

Figure 9: Contour plot of the (normalised) optical cross section of the retroreflector design of the present project, at receiver angle $\theta_r = \alpha$, the velocity aberration. The variation of the optical cross section with tilt angle in the direction required to broaden the reflected beam toward the receiver is shown. The red curve is the loci of optimal tilt angles $\theta_i^{(o)}(\alpha)$ that maximise the optical cross section of the retroreflector. Contours of the optical cross section corresponding to ten times the unity photon-count threshold are drawn to indicate the range of acceptable tilt angles.

the threshold, as shown in Figure 8. Yet this would not be optimal for many situations. If possible, tilting by the optimal angles shown by the curve in Figure 9 would give a higher photon count. To this end, the calculated values of the optimal tilt angles $\theta_i^{(o)}(\alpha)$ are listed in Table 2.

The tolerance for the direction of the retroreflector tilt axis is quite large, as shown in Figure 10. Denoting the azimuthal error of the tilt axis direction by φ_t, it can be seen from the figure that if the tilt angle magnitude is optimal (that is, $\theta_i = \theta_i^{(o)}(\alpha)$) then the unity photon-count threshold is exceeded for all expected velocity aberration values when $\varphi_t \lesssim 70°$. This wide tolerance for the unity threshold is much larger than the tolerance required to meet the $10\times$ threshold. At the higher threshold the tolerance on the orientation error is $\varphi_t \lesssim 25°$.

Table 2: Values of the optimum retroreflector tilt angles, $\theta_i^{(o)}$, (in degrees) as a function of velocity aberration, α, (in arcsec) for the current retroreflector design.

α	$\theta_i^{(o)}$	α	$\theta_i^{(o)}$	α	$\theta_i^{(o)}$	α	$\theta_i^{(o)}$
0.000	0.0000	7.000	8.8510	8.714	15.030	10.429	19.280
5.429	0.0000	7.143	9.4735	8.857	15.442	10.571	19.584
5.571	0.9243	7.286	10.072	9.000	15.842	10.714	19.875
5.714	1.8964	7.429	10.649	9.143	16.229	10.857	20.161
5.857	2.8187	7.571	11.204	9.286	16.605	11.000	20.444
6.000	3.6959	7.714	11.740	9.429	16.970	11.143	20.703
6.143	4.5322	7.857	12.256	9.571	17.335	11.286	20.967
6.286	5.3304	8.000	12.756	9.714	17.682	11.429	21.235
6.429	6.0945	8.143	13.242	9.857	18.022	11.571	21.488
6.571	6.8273	8.286	13.715	10.000	18.351	11.714	21.722
6.714	7.5319	8.429	14.166	10.143	18.671	11.857	21.971
6.857	8.2109	8.571	14.605	10.286	18.983	12.000	22.199

4.2.2 Point ahead ranging

Pointing the transmitter ahead of the apparent position of the satellite to allow for the time of flight of the laser pulse is often done when the return signal needs to be maximised; as in the case of uncooperative targets, for example. The size of the point-ahead angle, $\bar{\theta}_1$, can be calculated from the component, $\boldsymbol{v}'$, of the satellite's relative velocity that is orthogonal to the position vector, $\boldsymbol{r}$, of the satellite relative to the station. The satellite relative velocity, $\boldsymbol{v}$, is the time derivative of $\boldsymbol{r}$, and (from equation (14))

$$v' = |\boldsymbol{v} - (\boldsymbol{v} \cdot \hat{\boldsymbol{r}})\hat{\boldsymbol{r}}| = \frac{c\alpha}{2} \tag{26}$$

where $\hat{\boldsymbol{r}} = \boldsymbol{r}/|\boldsymbol{r}|$, and α is the velocity aberration. The one-way time of flight will be

$$\tau = \frac{r}{c} \tag{27}$$

and so the point-ahead angle can be written

$$\bar{\theta}_1 = \frac{v'\tau}{r} = \frac{\alpha}{2}; \tag{28}$$

that is, half the velocity aberration angle.

By the time the pulse has returned, the receiver will have rotated a further $\bar{\theta}_1$, and so will be at an angle $\theta_2 = \alpha$ to the returning light direction. The resulting relative change in receiver aperture area will be $(1 - \cos\theta_2) \approx 10^{-9}$, which is negligible.

These calculations neglect the effects of atmospheric propagation. Although the principles of the above discussion still hold, in practice the effects of atmospheric refraction must be included for accurate SLR. These calculations are beyond the scope of the present work. Further details of a standard, and long-standing, shell model of the atmosphere known as the Marini-Murray model are given in the review article by Degnan [5]. It is

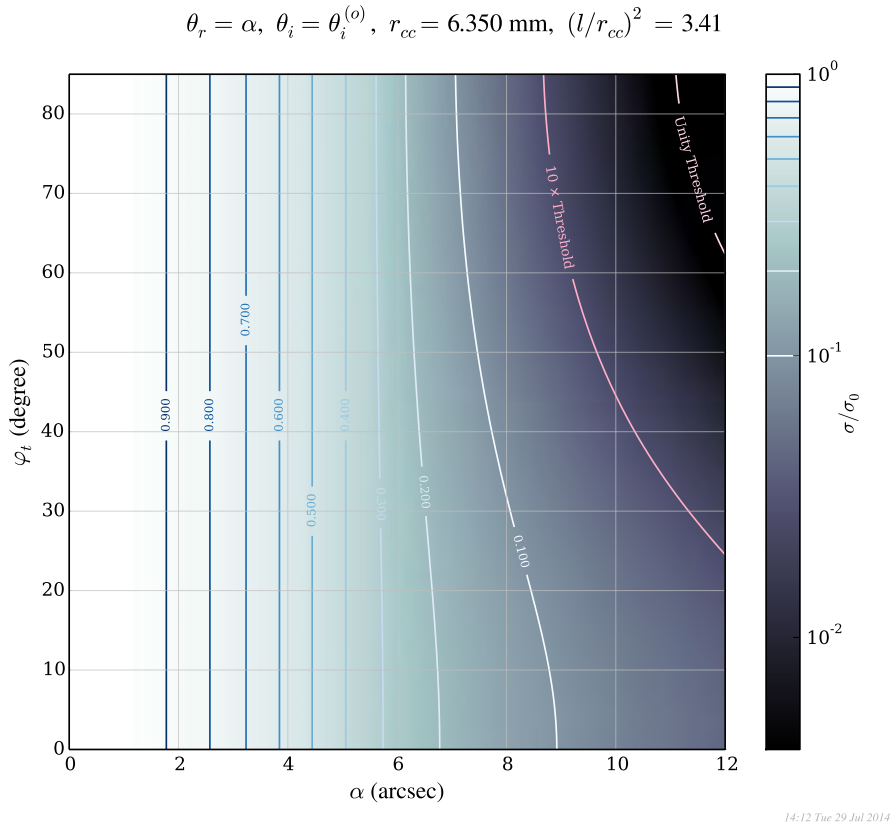

Figure 10: Contour plot of the (normalised) optical cross section of the retroreflector design of the present work, at receiver angle $\theta_r = \alpha$, the velocity aberration. The retroreflector tilt angle $\theta_i = \theta_i^{(o)}(\alpha)$, the optimum value for each value of the velocity aberration, but the *direction* of the tilt axis is in error by the azimuthal angle φ_t. The unity photon-count threshold contour is also plotted.

simply noted in passing that this particular model requires values of physical measures of the atmosphere—such as surface relative humidity, temperature, and pressure—to implement.

It should be noted that the point-ahead principle does not correct the velocity aberration, despite the direct relationship to it, since the direction of the part of the beam incident on the retroreflector is unchanged, and hence the reflected beam is still returned at the aberrated angle α. Nevertheless, it does ameliorate some of its effect by maximising the radiance of the beam striking the retroreflector. A point-ahead strategy is assumed in the photon-budget calculations in the present work.

4.3 Atmospheric and cirrus-cloud transmittance

The single-transit atmospheric transmittance, T_a, values were calculated using the MODTRAN 5 [16] computer software. The built-in mid-latitude summer and winter atmospheric models were used. The visibility component was set to the Rural Aerosol model

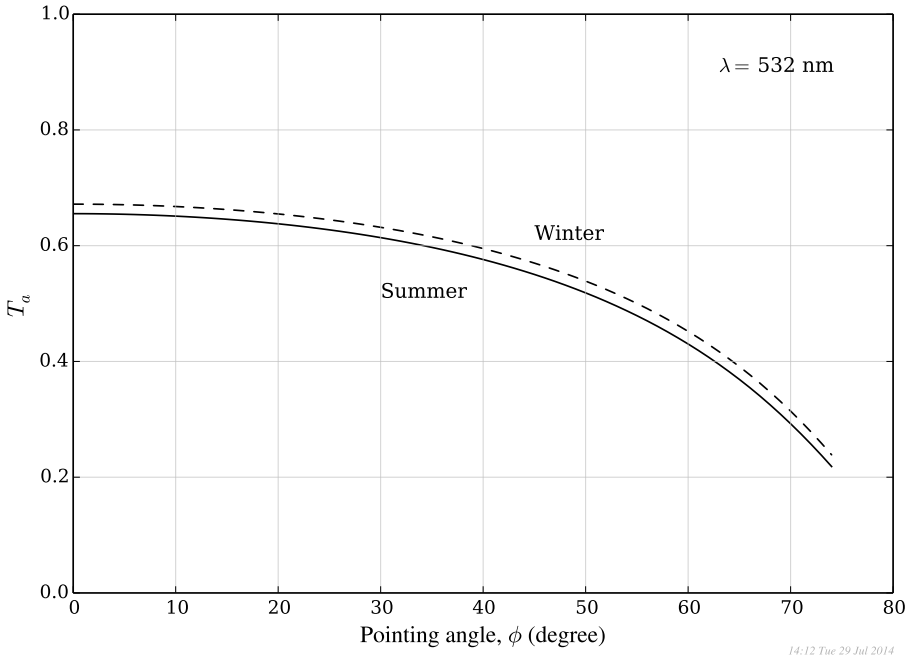

Figure 11: One-way atmospheric transmittance, T_a, calculated using MODTRAN 5 [16] for light of wavelength 532 nm and a bandwidth of 1 nm. Calculations were for the mid-latitude summer and winter atmospheric models, rural aerosol visibility of 23 km, and a ground altitude of 770 m above sea level.

with visibility of 23 km. The ground altitude above mean sea level was chosen to be 770 m, matching the Mount Stromlo station altitude. Light of wavelength 532 nm and with a bandwidth of 1 nm was modelled.

The resulting transmittance values for the useful range of zenith pointing angles are plotted in Figure 11. At any pointing angle, the summer atmosphere model gave a slightly smaller transmittance than the winter model at the same angle. The summer model transmittance values were therefore used in establishing the retroreflector tilt-angle tolerances.

The other transmittance parameter is the single-transit cirrus-cloud transmittance, T_c. Degnan [5] reported that this could be well represented by a value of approximately 0.8. This value is the mean cirrus-cloud transmittance at zenith when cirrus clouds are present, and has been found to be exceeded 75% of the time. The mean transmittance is lower at other angles; as low as 0.1 at 70° pointing angle. Yet it is found that no cirrus cloud is present 50% of the time, corresponding to a transmittance, $T_c = 1$. Accordingly, the representative value of $T_c = 0.8$ is used in the present calculations.

5 Photon budget

The results of a calculation of the photon count for the current system based on estimates of alignment tolerances are shown in Table 3. The table also lists the relevant parameter

values used. The retroreflector efficiency value, ρ, is based on the assumption of three reflections of the light from the silvered BK7 surfaces, for which a single-surface reflectance of 0.95 is assumed [2]. The other parameter values were discussed above.

The first two cases of the table show the photon counts, n_p, when the satellite is at the zenith ($\phi = 0$), and its velocity aberration is at its smallest for this pointing angle; that is, $\alpha\ (= \theta_r) = 9.88$ arcsec. With no tilting compensation, the photon count $n_p = 625.0$ which is adequate for pulse detection. The photon count increases approximately 25-fold, which is substantial, on applying the optimum tilt angle of $\theta_i = 18.2°$.

Cases 3–5 show the photon counts in the more marginal situation when the pointing angle, $\phi = 75°$ from the zenith. The velocity aberration varies between 4.37 arcsec and 10.92 arcsec, and without any tilt compensation the photon counts are respectively 184.1 and 0.279—the latter being barely sufficient for pulse detection, even in darkness. Application of the optimum tilt angle $\theta_i = 20.5°$ in the latter case yields a photon count of 21.22, which is now adequate for pulse detection.

6 Conclusion

In conclusion, it has been found that the retroreflector with ideal geometry should be tilted away from the SLR station in order to mitigate the effects of the velocity aberration. The optimum tilt angle varies with the size of the velocity aberration. At the maximum expected velocity aberration of 10.92 arcsec, a retroreflector tilt of $(20.5 \pm 17)°$ is required to exceed the unity photon-count threshold, with a tilt of $20.5°$ being optimal. The axis of the rotation is perpendicular to both the satellite (relative) velocity and the direction to the SLR station. The same tilt angle (and tolerance) can be used at lower velocity aberration values and still exceed the detection threshold. Nevertheless, a reduced tilt angle (according to the values in Table 2 and plotted in Figure 9) will give optimal photon counts. The most restricted range of acceptable tilt angles occurs when the velocity aberration is highest, and so this is the basis for the attitude control tolerance. Therefore, to just achieve the unity photon-count threshold in all situations, the attitude should be within $17°$ of the optimum tilt angle.

The retroreflector manufacturer's tolerance on the reflected beam direction of within 3 arcsec has been found to be equivalent to a tolerance of ± 1.2 arcsec on the cornercube dihedral angles. This amount of variation encompasses a wide range of far-field diffraction patterns that deviate significantly from that of the ideal geometry considered above. It is therefore recommended that each retroreflector be experimentally characterised to determine its diffraction pattern (and its optical cross section), and thence its associated optimal attitude-control strategy based on the methods described in the present work. The characterisation of the diffraction pattern could be a direct measurement as described, for example, by Boni *et al.* [7].

Table 3: Parameter values used in calculating the detected photon number, n_p. Only changes in parameter values have been recorded in moving between adjacent columns from left to right. Values marked "†" are simple estimates.

Parameter	Case 1	Case 2	Case 3	Case 4	Case 5	
λ	532 nm					Wavelength
E_t	20 mJ					Laser pulse energy
η_t	1.0†					Transmitter optics efficiency
a_t	0.5 m					Transmitter aperture outer radius
b_t	0.125 m					Transmitter aperture inner radius
Beam type	Flat top					
θ_d	8″					Beam full divergence angle
θ_1	0.085″					Beam direction error
a_r	0.5 m					Receiver aperture outer radius
b_r	0.125 m					Receiver aperture inner radius
η_r	0.35					Receiver optics efficiency
η_q	0.15					Detector efficiency
θ_r	9.88″		4.37″	10.925″		Receiver orientation error ($= \alpha$)
r_{cc}	0.635 cm					Retroreflector aperture radius
$(l/r_{cc})^2$	3.412					Retroreflector ratio
ρ	0.857					Retroreflector efficiency
θ_i	0°	18.2°	0°		20.5°	Retroreflector orientation error
ϕ	0°		75°			Pointing zenith angle
d	600 km		1626 km			Range
T_a	0.655		0.198			Atmospheric transmittance
T_c	0.8†					Cirrus cloud transmittance
G_T	1.22×10^{10}	1.22×10^{10}	1.25×10^{10}	1.25×10^{10}	1.25×10^{10}	Transmitter gain
σ	1.84×10^{3}	4.70×10^{4}	3.14×10^{5}	4.76×10^{2}	3.61×10^{4}	Reflector optical cross section
n_p	625.0	15,920.	184.1	0.279	21.22	Detected photon count

References

1. Stephenson, P. C. L. & Perejogin, V. (2011) SLR reflector photon-budget calculations for a single satellite reflector. Unpublished technical note.

2. Polyanskiy, M. N. (2014) Refractive index database, http://refractiveindex.info.

3. Smith, C. (2014) EOS Australia, Personal communication.

4. *Edmund Optics catalogue* (2014) http://www.edmundoptics.com/optics/prisms/retroreflection-prisms/mounted-n-bk7-corner-cube-retroreflectors/45-203. Accessed 25 July, 2014.

5. Degnan, J. J. (1993) Millimeter accuracy satellite laser ranging: A review, *in Contributions of Space Geodesy to Geodynamics: Technology*, Vol. 25 of *AGU Geodynamics Series*, pp. 133–162.

6. Otsubo, T., Kunimori, H., Noda, H., Hanada, H., Araki, H. & Katayama, M. (2011) Asymmetric dihedral angle offsets for large-size lunar laser ranging retroreflectors, *Earth Planets Space* **63**, e13–e16.

7. Boni, A., Cantone, C., Dell'Agnello, S., Delle Monache, G. O., Garattini, M., Intaglietta, N., Lops, C., Martini, M. & Porcelli, L. (2008) *Optical far field diffraction pattern test of laser retroreflectors for space applications in air and isothermal conditions at INFN-LNF*, Report LNF-08/26 (IR), Istituto Nazionale di Fisica Nucleare—Laboratori Nazionali di Frascati, Frascati.

8. Dell'Agnello, S., Delle Monache, G. O., Currie, D. G., Vittori, R., Cantone, C., Garattini, M., Boni, A., Martini, M., Lops, C., Intaglietta, N., Tauraso, R., Arnold, D., Pearlman, M., Bianco, G., Zerbini, S., Maiello, M., Berardi, S., Porcelli, L., Alley, C., McGarry, J., Sciarretta, C., Luceri, V. & Zagwodzki, T. (2011) Creation of the new industry-standard space test of laser retroreflectors for the GNSS and LAGEOS, *Advances in Space Reseach* **47**(5), 822–842.

9. Arnold, D. A. (1979) *Method of calculating retroreflector-array transfer functions*, Special Report 382, Smithsonian Astrophysical Observatory.

10. Campbell, J. P. & DeShazer, L. G. (1969) Near fields of truncated-Gaussian apertures, *Journal of the Optical Society of America* **59**, 1427–1429.

11. Shealy, D. L. & Hoffnagle, J. A. (2006) Laser beam shaping profiles and propagation, *Applied Optics* **45**(21), 5118–5131.

12. Minott, P. O. (1974) *Design of retrodirector arrays for laser ranging of satellites*, Technical Report NASA TM-X-723-74-122, Goddard Space Flight Center.

13. Nugent, L. J. & Condon, R. J. (1966) Velocity aberration and atmospheric refraction in satellite laser communication experiments, *Applied Optics* **5**(11), 1832–1837.

14. Resnick, R. (1968) *Introduction to Special Relativity*, John Wiley & Sons.

15. Minott, P. O., Zagwodzki, T. W., Varghese, T. & Seldon, M. (1993) *Prelaunch Optical Characterization of the Laser Geodynamic Satellite (LAGEOS 2)*, NASA Technical Paper 3400, NASA, Goddard Space Flight Centre.

16. Spectral Sciences Inc. (2004) *MODTRAN®5*, Spectral Sciences Inc. Version 5.2.3.

17. Goodman, J. W. (1996) *Introduction to Fourier Optics*, second edn, McGraw-Hill.

18. Minott, P. O. (1972) *Analysis of requirements for GEOS-C laser cube-corner reflector panels*, Technical Report X-524-72-33, Goddard Space Flight Center. NASA-TM-X-65862.

19. Song, G. H. (1987) *Single-color laser ranging with a cube-corner-retroreflector array*, Technical Report EOSL No. 87-004, National Aeronautics & Space Administration, Goddard Space Flight Center.

20. Smith, R. C. & Marsh, J. S. (1974) Diffraction patterns of simple apertures, *Journal of the Optical Society of America* **64**(6), 798–803.

Appendix A Tilted cornercube retroreflector far-field diffraction pattern

The optical cross section of a retroreflector illuminated by a uniform, coherent light across its aperture is

$$\sigma = 4\pi d^2 \rho\, U^2(\bar{x}, \bar{y}) \tag{A1}$$

where ρ is the reflectance of the retroreflector and $U(\bar{x}, \bar{y})$ is the electric field amplitude distribution from the retroreflector on a plane with coordinates $(\bar{x}, \bar{y})$, at the observation distance d. In the present case, the distance d is much larger than the retroreflector aperture (a circle of radius r_{cc}), and so $U(\bar{x}, \bar{y})$ can be represented accurately by the far-field (Fraunhofer) diffraction distribution [17]

$$U(\bar{x}, \bar{y}) = \frac{1}{id\lambda} \exp\left\{ i \frac{k}{2d} \left[2d^2 + \left(\bar{x}^2 + \bar{y}^2 \right) \right] \right\} \iint_{\Omega} \exp\left[-i \frac{k}{d} \left(\bar{\xi}\bar{x} + \bar{\eta}\bar{y} \right) \right] d\bar{\xi}\, d\bar{\eta} \tag{A2}$$

where the integral is over the effective aperture, Ω, of the retroreflector, with Cartesian pupil-plane coordinates $(\bar{\xi}, \bar{\eta})$, and where the $\bar{\xi}$-axis is parallel to the $\bar{x}$-axis. The wavelength of the monochromatic light is λ, and $k = \frac{2\pi}{\lambda}$ is the propagation number.

The shape of the aperture, and hence the limits of integration, are affected by the tilt of the retroreflector. In the case of a circular aperture tilted by angle θ_i from normal incidence of the light, the aperture width in one dimension—without loss of generality along the $\bar{\xi}$-axis—is reduced by a factor of $\cos\theta_i$. Additionally, in cornercube retroreflectors there is a lateral displacement [9, 18] of the image of the aperture which in turn leads to a truncation of the effective aperture. If the depth of the cornercube retroreflector is l, and if the retroreflector front surface is not recessed, then the lateral displacement is $l \tan|\theta'|$, where θ' is the refracted angle of the light ray to the surface normal in the cornercube. This angle can be calculated from Snel's law, and is

$$\theta' = \sin^{-1}\left(\frac{\sin\theta_i}{n} \right) \tag{A3}$$

where n is the refractive index of the solid cornercube material. In the case of a hollow cornercube, $n = 1$ and so $\theta' = \theta_i$. Otherwise θ' is in general less than the tilt angle θ_i. The resulting expressions describing the shape of the effective aperture of the tilted cornercube retroreflector are then

$$\bar{\xi} = \pm \bar{F}(\bar{\eta}), \quad |\bar{\eta}| \le \bar{\mu} \tag{A4}$$

where

$$\bar{F}(\bar{\eta}) = \cos\theta_i \left(\sqrt{r_{cc}^2 - \bar{\eta}^2} - l \tan|\theta'| \right) \tag{A5}$$

and

$$\bar{\mu} = \left| \bar{F}^{-1}(0) \right| = r_{cc} \sqrt{1 - (l/r_{cc})^2 \tan^2\theta'}. \tag{A6}$$

Note that in the untilted case, $\theta_i = \theta' = 0$ and

$$\bar{F}(\bar{\eta})|_{\theta_i = 0} = \sqrt{r_{cc}^2 - \bar{\eta}^2} \tag{A7}$$

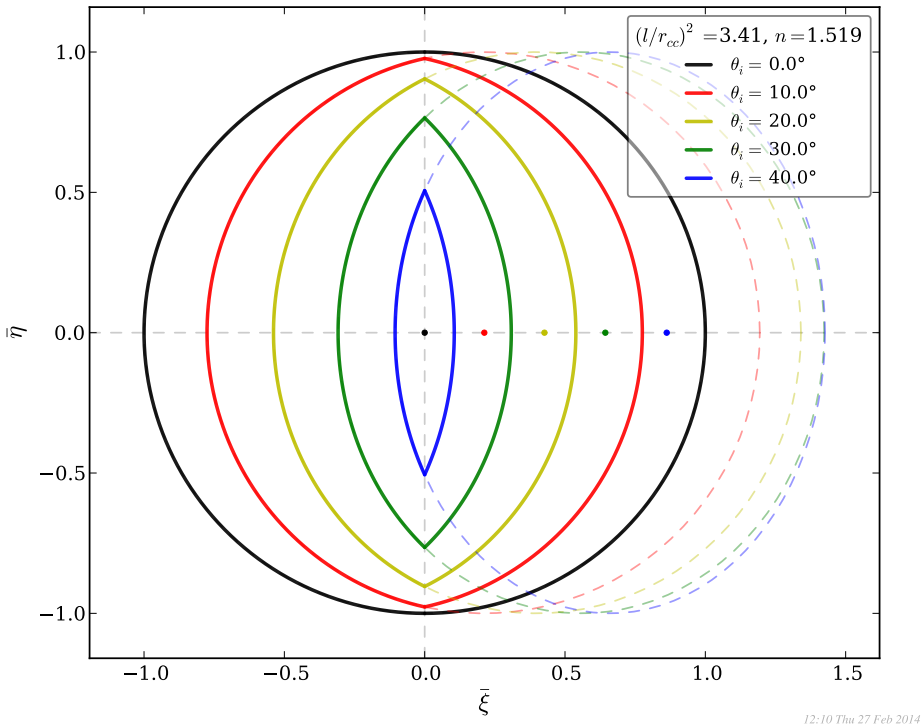

Figure A1: The apparent aperture shapes (solid lines) of a unit-radius, solid N-BK7 cornercube retroreflector at a number of different tilt angles, θ_i. The retroreflector has been tilted about an axis parallel to the η-axis. The outline of the circular aperture, foreshortened due to the retroreflector tilt are drawn in dashed lines. The effective apertures are further restricted due to the lateral displacement of the reflected light, by an amount that increases with tilt angle. The effective aperture is equal to the actual aperture only in the untilted ($\theta_i = 0°$) case, shown in black.

is the equation of a circular aperture of radius r_{cc}, as required. Figure A1 shows plots of the effective aperture outlines ($\bar{\xi} = \pm\bar{F}(\bar{\eta})$) of a unit-radius retroreflector at various amounts of tilt. Also shown are the corresponding projected aperture outlines—the considerable effect of the image lateral displacement on the effective aperture can be clearly seen.

The evaluation of the above diffraction integral can be greatly simplified by a change in variables. Firstly, let

$$(x, y) = \frac{kr_{cc}}{d}(\bar{x}, \bar{y}) \tag{A8}$$

and then make use of the normalised pupil-plane coordinates

$$(\xi, \eta) = \frac{1}{r_{cc}}(\bar{\xi}, \bar{\eta}). \tag{A9}$$

With these changes to the variables, the above expression for the electric-filed distribution at the observation plane may be written

$$U^2(x, y) = U(x, y)U^*(x, y) = \frac{r_{cc}^4}{d^2\lambda^2}W^2(x, y) \tag{A10}$$

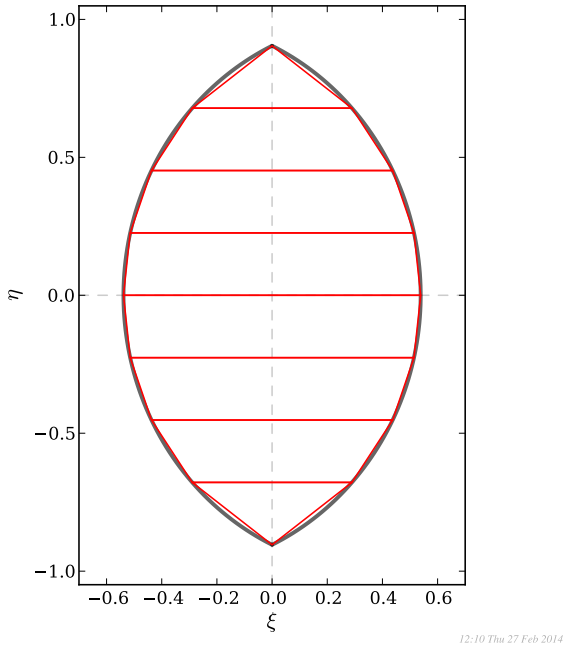

Figure A2: The effective aperture (black) of a unit-radius aperture tilted $\theta_i = 20°$ ($(l/r_{cc})^2 = 3.41$, $n = 1.519$), and an example set of $N = 8$ equal-height trapezoids used to approximate the effective aperture in the numerical evaluation of the diffraction integral. In practice, a much larger set of trapezoids is used.

where

$$W(x,y) = \int_{-\mu}^{\mu} \int_{-F(\eta)}^{F(\eta)} \exp\left[-i\left(\xi x + \eta y\right)\right] \, d\xi \, d\eta \tag{A11}$$

and where

$$\mu = \bar{\mu}/r_{cc} = \sqrt{1 - (l/r_{cc})^2 \tan^2\theta'} \tag{A12}$$

$$F(\eta) = \bar{F}(\eta)/r_{cc} = \cos\theta_i \left(\sqrt{1-\eta^2} - \tfrac{l}{r_{cc}} \tan|\theta'|\right). \tag{A13}$$

Note that when $(x,y) = (0,0)$—that is, the receiver orientation error, $\theta_r = 0$—the integrals can be evaluated analytically, and so may be written

$$W(0,0) = 2\cos\theta_i \left[\sin^{-1}\mu - \tfrac{l}{r_{cc}}\mu \tan|\theta'|\right] = \pi\kappa(\theta_i). \tag{A14}$$

The optical cross-section is then

$$\sigma\Big|_{\theta_r=0} = \rho\frac{4\pi}{\lambda^2}\left[A_{cc}\kappa(\theta_i)\right]^2. \tag{A15}$$

In the more general case where (x,y) can take any values, the above double integral can be efficiently numerically evaluated by first approximating the integration domain (that is, the normalised effective aperture) by a sequence of N adjacent trapezoids [19] as shown in Figure A2. Simple analytic expressions for the above diffraction integral over a trapezoid are known [20], and the sloped edges of the trapezoids better approximate

the edges of the aperture, $\xi = \pm F(\eta)$ as the number, N, of trapezoids is increased. The resulting approximation becomes

$$W(x,y) \approx \sum_{m=1}^{N} I_m(x,y) \tag{A16}$$

where the diffraction integral for the m-th trapezoid is

$$I_m(x,y) = \begin{cases} \frac{2h}{x}\left\{\sin(\xi_m x + \eta_m y)\,\mathrm{sinc}(h[y+\alpha_m x]) \right. \\ \qquad \left. + \sin(\xi_m x - \eta_m y)\,\mathrm{sinc}(h[y-\alpha_m x])\right\} & x \neq 0 \\ 4h\left\{\xi_m \cos(\eta_m y)\,\mathrm{sinc}(hy) \right. \\ \qquad \left. + \alpha_m \eta_m \,\mathrm{sinc}(2\eta_m y)\,[\cosh(y/2) - \mathrm{sinc}(hy)]\right\} & x = 0 \end{cases} \tag{A17}$$

where

$$\mathrm{sinc}(\omega) = \begin{cases} \frac{\sin(\omega/2)}{\omega/2} & \omega \neq 0 \\ 1 & \omega = 0 \end{cases} \tag{A18}$$

$$\xi_m = \tfrac{1}{2}\left[F(mh) + F((m-1)h)\right] \tag{A19}$$

$$\eta_m = \left(m - \tfrac{1}{2}\right) h \tag{A20}$$

$$\alpha_m = \tfrac{1}{2}\left[F(mh) - F((m-1)h)\right] \tag{A21}$$

$$h = \mu/N. \tag{A22}$$

The accuracy of the above approximation improves with increasing number, N, of trapezoidal divisions. It also depends on the shape of the effective aperture, and hence on the retroreflector tilt. Figure A3 shows plots of the relative error of the numerical approximation, calculated over a range of values of N. It can be seen that the relative error follows a power-law relation

$$\epsilon = k_1 N^{-k_2} \tag{A23}$$

for large values of N, where the values of the parameters k_i depend on the tilt angle. In the present work, N was chosen to be 1,500 in order to give values correct to at least five significant figures, at any tilt angle.

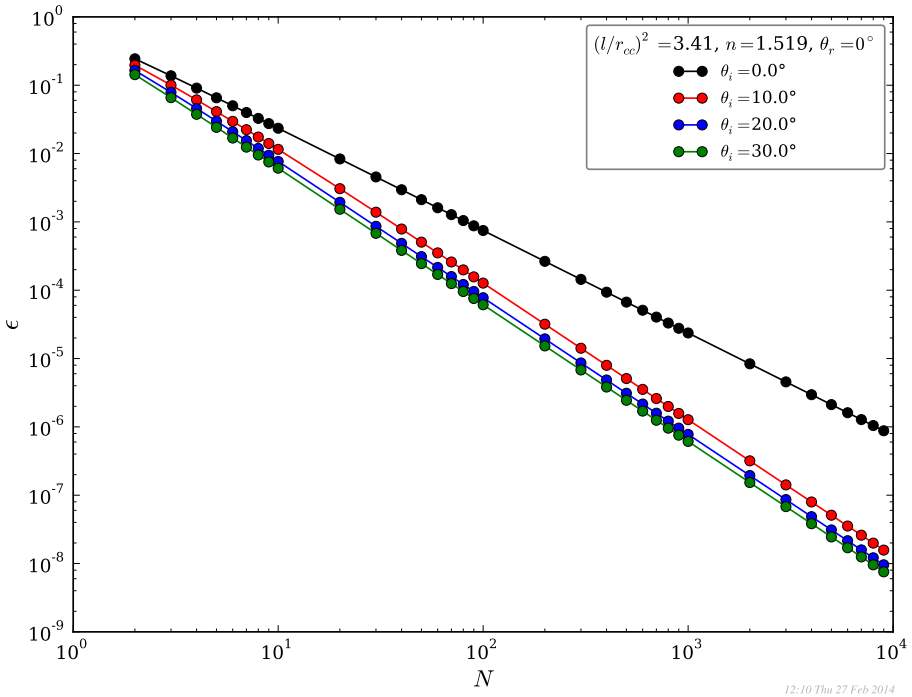

Figure A3: Relative errors, ϵ, in the numerical approximation calculation of the optical cross section on axis ($\theta_r = 0°$), for which an explicit expression is known (equation (A15)).

Appendix B Spoiled cornercube retroreflector ray deflection

Let the 3-dimensional coordinate system be represented by the three orthonormal vectors $\hat{\boldsymbol{\mu}}_l$, where $l = 1, 2, 3$. Without loss of generality, the three planar reflecting faces of a cornercube can be described by the three unit vectors that are each normal to one of the faces, and by fixing the apex of the cornercube at the origin. The three unit normals can be written

$$\hat{\boldsymbol{\mu}}'_i = \sum_l \sigma_{il} \hat{\boldsymbol{\mu}}_l \tag{B1}$$

where $i = 1, 2, 3$ and the scalar coefficients, σ_{il}, are the Cartesian coordinates. In the special case of a perfect cornercube whose faces are all mutually orthogonal, the unit normal vectors are equal to the basis vectors so that

$$\sigma_{il} = \delta_{il} \tag{B2}$$

where δ_{il} is the Krönecker delta function. More generally, for an imperfect cornercube

$$\sigma_{il} = \hat{\boldsymbol{\mu}}'_i \cdot \hat{\boldsymbol{\mu}}_l. \tag{B3}$$

The cosine of the dihedral angle, θ_{ij}, between adjacent faces whose unit normals are $\hat{\boldsymbol{\mu}}'_i$ and $\hat{\boldsymbol{\mu}}'_j$ will be

$$\begin{aligned} \epsilon_{ij} &= \hat{\boldsymbol{\mu}}'_i \cdot \hat{\boldsymbol{\mu}}'_j \\ &= \sum_{l,m} \sigma_{il}\sigma_{jm} \hat{\boldsymbol{\mu}}_l \cdot \hat{\boldsymbol{\mu}}_m \\ &= \sum_l \sigma_{il}\sigma_{jl}. \end{aligned} \tag{B4}$$

In matrix notation, if $[\boldsymbol{\epsilon}]_{ij} = \epsilon_{ij}$ and $[\boldsymbol{\sigma}]_{ij} = \sigma_{ij}$ then

$$\boldsymbol{\epsilon} = \boldsymbol{\sigma}\boldsymbol{\sigma}^T. \tag{B5}$$

Note that the diagonal elements

$$\epsilon_{ii} = 1 = \sum_l \sigma_{il}^2 \tag{B6}$$

which is consistent with the normalisation of the $\hat{\boldsymbol{\mu}}'_i$. A perfect cornercube will have $\epsilon_{ij} = 0$ if $i \neq j$.

If a unit vector $\hat{\boldsymbol{m}} = (\alpha_1, \alpha_2, \alpha_3)$ represents the direction of a ray striking surface i (that is, the face with unit normal $\hat{\boldsymbol{\mu}}'_i$) then the direction of the reflected ray will be

$$\hat{\boldsymbol{m}}_i = \hat{\boldsymbol{m}} - 2(\hat{\boldsymbol{m}} \cdot \hat{\boldsymbol{\mu}}'_i)\hat{\boldsymbol{\mu}}'_i \tag{B7}$$

by the usual law of reflection. This reflected ray will in turn be reflected by the other two faces. The order in which the ray strikes the faces will depend on the lateral placement of the original ray. In general the order of the three faces can be denoted i–j–k, where

$i \neq j \neq k$. The above expression for the single reflection can be repeatedly applied twice to give the retro-reflected ray direction

$$\begin{aligned}\hat{\boldsymbol{m}}_k = \hat{\boldsymbol{m}} &- 2\sum_l (\hat{\boldsymbol{m}} \cdot \hat{\boldsymbol{\mu}}'_l)\hat{\boldsymbol{\mu}}'_l \\ &+ 4\left[\epsilon_{ij}(\hat{\boldsymbol{m}} \cdot \hat{\boldsymbol{\mu}}'_i)\hat{\boldsymbol{\mu}}'_j + \epsilon_{ik}(\hat{\boldsymbol{m}} \cdot \hat{\boldsymbol{\mu}}'_i)\hat{\boldsymbol{\mu}}'_k + \epsilon_{jk}(\hat{\boldsymbol{m}} \cdot \hat{\boldsymbol{\mu}}'_j)\hat{\boldsymbol{\mu}}'_k\right] \\ &- 8\epsilon_{ij}\epsilon_{jk}(\hat{\boldsymbol{m}} \cdot \hat{\boldsymbol{\mu}}'_i)\hat{\boldsymbol{\mu}}'_k. \end{aligned} \quad \text{(B8)}$$

In the special case of a perfect cornercube the ϵ_{ij} terms vanish and the expression simplifies to $\hat{\boldsymbol{m}}_k = -\hat{\boldsymbol{m}}$, as expected. For an imperfect cornercube the terms involving a dot product can be written in terms of the basis vectors by using equation (B1), so that

$$(\hat{\boldsymbol{m}} \cdot \hat{\boldsymbol{\mu}}'_i)\hat{\boldsymbol{\mu}}'_j = \sum_{l,m} \alpha_l \sigma_{il}\sigma_{jm}\hat{\boldsymbol{\mu}}_m, \quad \text{(B9)}$$

and finally

$$\begin{aligned}\hat{\boldsymbol{m}}_k = \hat{\boldsymbol{m}} &- \sum_{l,m} \alpha_l \hat{\boldsymbol{\mu}}_m \times \\ &\left\{2\sum_n \sigma_{nl}\sigma_{nm} - 4\left[\epsilon_{ij}\sigma_{il}\sigma_{jm} + \epsilon_{ik}\sigma_{il}\sigma_{km} + \epsilon_{jk}\sigma_{jl}\sigma_{km}\right] + 8\epsilon_{ij}\epsilon_{jk}\sigma_{il}\sigma_{km}\right\}. \end{aligned} \quad \text{(B10)}$$

The deviation of the retro-reflected ray from the perfect case is then

$$\varphi = \cos^{-1}(-\hat{\boldsymbol{m}} \cdot \hat{\boldsymbol{m}}_k). \quad \text{(B11)}$$

In order to restrict the orientation of the cornercube, while maintaining the three degrees of freedom of its construction that are its dihedral angles, the σ_{ij} are assumed to symmetrical; that is, $\sigma_{ij} = \sigma_{ji}$. If the normalisation constraint of the $\hat{\boldsymbol{\mu}}'_i$ is also considered, there remain just three independent components of the $\boldsymbol{\sigma}$ matrix, so that it may be written

$$\boldsymbol{\sigma} = \begin{pmatrix} \sqrt{1-(\sigma_a^2+\sigma_b^2)} & \sigma_a & \sigma_b \\ \sigma_a & \sqrt{1-(\sigma_a^2+\sigma_c^2)} & \sigma_c \\ \sigma_b & \sigma_c & \sqrt{1-(\sigma_b^2+\sigma_c^2)} \end{pmatrix} \quad \text{(B12)}$$

where $\sigma_a = \sigma_{12}$, $\sigma_b = \sigma_{13}$ and $\sigma_c = \sigma_{23}$. It follows that the matrix of the dihedral angle cosines, $\boldsymbol{\epsilon}$, is also symmetric with independent elements

$$\begin{aligned} \epsilon_a = \epsilon_{12} &= \sigma_a\sqrt{1-(\sigma_a^2+\sigma_b^2)} + \sigma_a\sqrt{1-(\sigma_a^2+\sigma_c^2)} + \sigma_b\sigma_c \\ \epsilon_b = \epsilon_{13} &= \sigma_b\sqrt{1-(\sigma_a^2+\sigma_b^2)} + \sigma_a\sigma_c + \sigma_b\sqrt{1-(\sigma_b^2+\sigma_c^2)} \\ \epsilon_c = \epsilon_{23} &= \sigma_a\sigma_b + \sigma_c\sqrt{1-(\sigma_a^2+\sigma_c^2)} + \sigma_c\sqrt{1-(\sigma_b^2+\sigma_c^2)} \end{aligned} \quad \text{(B13)}$$

The problem at hand is to calculate the ray deviation, φ, for any given values of the $(\epsilon_a, \epsilon_b, \epsilon_c)$. To do this, the values of the $(\sigma_a, \sigma_b, \sigma_c)$ must be found from the $(\epsilon_a, \epsilon_b, \epsilon_c)$ using

the nonlinear equations (B13). This can be done numerically using any of a number of standard nonlinear root-finding methods, with the first-order approximation

$$(\sigma_a, \sigma_b, \sigma_c) \approx (\epsilon_a, \epsilon_b, \epsilon_c)/2 \tag{B14}$$

as the initial estimate of the solution. The value of the ray deviation angle, φ, can then be calculated using equations (B11) and (B10).

A further consideration in calculating the retro-reflected ray direction in the case of a solid cornercube is the refraction at the front surface, both on entry and exit of the ray. Let the front surface normal be $\hat{\boldsymbol{\mu}}_n$ and let it be fixed at

$$\hat{\boldsymbol{\mu}}_n = (\hat{\boldsymbol{\mu}}_1 + \hat{\boldsymbol{\mu}}_2 + \hat{\boldsymbol{\mu}}_3)/\sqrt{3}. \tag{B15}$$

The incoming ray is $\hat{\boldsymbol{m}} = \alpha_1\hat{\boldsymbol{\mu}}_1 + \alpha_2\hat{\boldsymbol{\mu}}_2 + \alpha_3\hat{\boldsymbol{\mu}}_3$, where for a normal-incident ray $\alpha_1 = \alpha_2 = \alpha_3 = -1/\sqrt{3}$. The ray will be refracted to a new direction $\boldsymbol{m}'$ by Snel's law

$$n\boldsymbol{m}' = \hat{\boldsymbol{m}} - \Gamma\hat{\boldsymbol{\mu}}_n \tag{B16}$$

where n is the refractive index of the cornercube material, and

$$\Gamma = \sqrt{n^2 - 1 + (\hat{\boldsymbol{\mu}}_n \cdot \hat{\boldsymbol{m}})^2} + \hat{\boldsymbol{\mu}}_n \cdot \hat{\boldsymbol{m}}. \tag{B17}$$

Similarly, the return ray, $\hat{\boldsymbol{m}}'_k$, will be refracted by the same surface to give the ray direction

$$\boldsymbol{m}_k = n\hat{\boldsymbol{m}}'_k + \Gamma'\hat{\boldsymbol{\mu}}_n \tag{B18}$$

where

$$\Gamma' = \sqrt{1 - n^2 + n^2(\hat{\boldsymbol{\mu}}_n \cdot \hat{\boldsymbol{m}}'_k)^2} - n(\hat{\boldsymbol{\mu}}_n \cdot \hat{\boldsymbol{m}}'_k). \tag{B19}$$

Note that the refracted ray directions, $\boldsymbol{m}'$ and $\boldsymbol{m}_k$, calculated by the above expressions are not normalised.

It is now possible to determine numerically the value of the dihedral angle cosine ϵ_a, say, as a function of ϵ_b and ϵ_c that gives any particular values of the retro-reflected ray deviation φ. In the present case, the ray deviation is $\varphi = 3$ arcsec and the solid cornercube material N-BK7 has a refractive index $n = 1.519$. If the dihedral angle θ_a differs from $\pi/2$ by β_a then

$$\epsilon_a = \cos(\pi/2 + \beta_a) \tag{B20}$$

with similar expressions for ϵ_b and ϵ_c. By considering the maximum ray deviation φ_{max} from each of the three unique permutations of the reflecting face order i–j–k, the two extreme values of β_a as a function of the other dihedral angle errors β_b and β_c can be found that give the prescribed maximum ray deviation. The results of these calculations are shown plotted in Figure B1. Here a normally incident ray is assumed. It can be seen that in the present case, the corresponding tolerance on the dihedral angles is ± 1.2 arcsec.

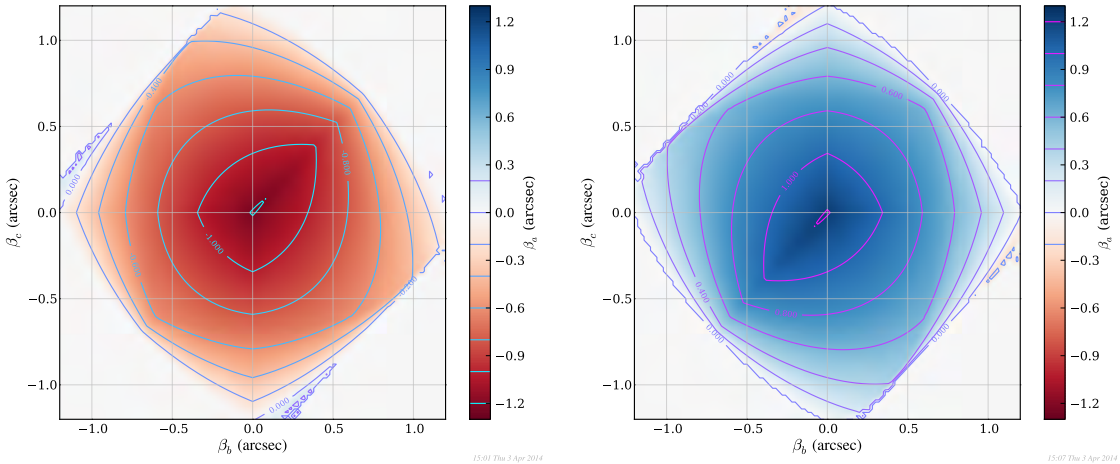

Figure B1: Dihedral angle error β_a as a function of the other dihedral angle errors, β_b and β_c, that gives a return narrow-beam deflection equal to the tolerance (3 arcsec) specified by the manufacturer of the cornercube retroreflector considered in the present work. The lower and upper limits are shown respectively in the left-hand and right-hand plots. Values of the dihedral angle pair (β_b, β_c) that lie outside the $\beta_a = 0$ contour lines will always exceed the ray-deviation tolerance. The dihedral angles therefore fall within approximately 1.2 arcsec of the (designed) right angles.

DEFENCE SCIENCE AND TECHNOLOGY GROUP DOCUMENT CONTROL DATA				1. DLM/CAVEAT (OF DOCUMENT)
2. TITLE Satellite Laser Ranging Photon-Budget Calculations for a Single Satellite Cornercube Retroreflector: Attitude Control Tolerance				3. SECURITY CLASSIFICATION (FOR UNCLASSIFIED REPORTS THAT ARE LIMITED RELEASE USE (L) NEXT TO DOCUMENT CLASSIFICATION) Document (U) Title (U) Abstract (U)
4. AUTHORS Philip C L Stephenson				5. CORPORATE AUTHOR Defence Science and Technology Group PO Box 1500 Edinburgh, South Australia 5111, Australia
6a. DST GROUP NUMBER DST-Group–TR–3172	6b. AR NUMBER 016–445	6c. TYPE OF REPORT Technical Report	7. DOCUMENT DATE November, 2015	
8. FILE NUMBER 2014/1095757/1	9. TASK NUMBER N/A	10. TASK SPONSOR N/A	11. No. OF PAGES 29	12. No. OF REFS 20
13. DST Group Publications Repository http://dspace.dsto.defence.gov.au/dspace/			14. RELEASE AUTHORITY Chief, National Security and ISR Division	
15. SECONDARY RELEASE STATEMENT OF THIS DOCUMENT *Approved for Public Release* OVERSEAS ENQUIRIES OUTSIDE STATED LIMITATIONS SHOULD BE REFERRED THROUGH DOCUMENT EXCHANGE, PO BOX 1500, EDINBURGH, SOUTH AUSTRALIA 5111				
16. DELIBERATE ANNOUNCEMENT No Limitations				
17. CITATION IN OTHER DOCUMENTS No Limitations				
18. DST GROUP RESEARCH LIBRARY THESAURUS Satellite attitude, Laser range finding, Retroreflectors, Diffraction, Geometrical optics				

19. ABSTRACT

The effect of cornercube retroreflector orientation on satellite laser ranging (SLR) detected photon counts is examined. It is found that a retroreflector tilt can ameliorate the effects of the satellite velocity aberration by broadening the reflected beam through diffraction. The optimal tilt angle, away from the SLR station, can be up to approximately 20.5° for the present retroreflector design. The size and direction of the tilt angle depend on the satellite velocity relative to the SLR station, and the direction of the satellite from the SLR station. The required attitude control tolerance is to within 17° of the optimal attitude control strategy determined in the present work. A pre-launch measurement of the reflectance (diffraction) pattern of each retroreflector is recommended to take account of the significant likely manufacturing variation.